2022

Experimental Investigation of R454C as a Replacement for R410A in a Residential Heat Pump Split System

Weigang Hou

Hafez Raeisi Fard

Larry Burns

Eckhard A. Groll

Davide Ziviani

See next page for additional authors

Authors

Weigang Hou, Hafez Raeisi Fard, Larry Burns, Eckhard A. Groll, Davide Ziviani, and James E. Braun

Experimental Investigation of R454C as a Replacement for R410A in a Residential Heat Pump Split System

Weigang Hou[1*], Hafez Raeisi Fard[2], Larry Burns[2], Eckhard A. Groll[1], Davide Ziviani[1], James E. Braun[1]

[1] Ray W. Herrick Laboratories, Purdue University
177 S Russell Street, West Lafayette, IN, 47907-2099, USA
hou111@purdue.edu, groll@purdue.edu, dziviani@purdue.edu, jbraun@purdue.edu

[2] Carrier Corporation, 7310 W Morris St., Indianapolis, IN, 46231, USA
hafez.fard@carrier.com, larry.burns@carrier.com

*corresponding author

ABSTRACT

In recent years, environmental concerns accelerated the quest for alternative low-GWP working fluids to replace current HFCs and their blends. However, trade-offs exist between desired performance characteristics and flammability. In this paper, a fully-instrumented 10.5 kW (3RT) residential heat pump split system has been utilized to conduct experimental comparisons between R410A and R454C under both heating and cooling conditions. As R454C has a lower volumetric capacity compared to R410A, a compressor with larger volume displacement was selected for R454C in an attempt to obtain similar capacity as R410A system. A wide range of experimental data has been collected by varying condensing and evaporating temperatures as well as the superheating degree. Moreover, charge sensitivity tests were carried out to investigate the effect of charge on cycle operation, component sizing and system performance. The results showed that, in heating mode, the heating capacity and the system heating COP obtained with R454C were about 6.56~7.66% and approximately 8.37~11.36% lower than the values measured with R410A, respectively. In cooling mode, the cooling capacity and the system cooling COP with R454C were approximately 2.45~10.55% and 6.90~21.23% lower than those obtained with R410A, respectively. The experimental results highlighted the need for optimizing heat exchanger areas as well as compressor displacement to achieve the desired nominal capacity and system performance with a high-glide refrigerant mixture.

1. INTRODUCTION

According to recent predictions, without a sharp decline in greenhouse gas emissions by 2030, global warming will surpass 1.5°C between 2030 and 2052, leading to negative and irreversible effects on the most fragile ecosystems and human societies (Masson-Delmotte et al., 2018). It is well known that HVAC&R systems contribute to global warming primarily through refrigerant leaks. In 2014, the European Union (EU) approved the F-Gas Regulation (No 517/2014) and established guidelines for hydrofluorocarbons (HFCs) management. In particular, F-Gas Regulation prohibited the use of fluorinated refrigerants with global warming potential (GWP$_{100yr}$) over 750 used in single split air-conditioning systems from 2025, which will exclude R410A and other commonly used high GWP refrigerants (European Commission, 2014). The American Innovation and Manufacturing (AIM) Act, which was enacted in 2020, will direct the U.S. Environmental Protection Agency (EPA) to phase down the production and consumption of HFCs to 85% of their baseline levels by 2036 through an allowance allocation and trading program (EPA, 2021). This HFCs allowance rule will further restrict the entities that import HFCs and HFC blends. Conventional refrigerants such as R134a, R404A, and R410A, which are widely used in many residential air conditioning (RAC) applications, are considered as high GWP refrigerants and are being phased out (Godwin, D. S., & Ferenchiak, R., 2020). Some of the replacement candidates include hydrofluoroolefins (HFOs) and mixtures of HFCs/HFOs as well as natural refrigerants (*e.g.*, hydrocarbons). HFC/HFO refrigerant mixtures have the potential of mitigating the flammability concerns of some pure HFOs and hydrocarbons, while meeting the GWP requirements set by regulatory entities and maintaining a performance similar to their HFC predecessors. Experimental system-level investigations of these mixtures have shown that they may be considered as viable 'drop-in' substitutes (Mota-Babiloni et al., 2015). To achieve maximum performance benefits and energy savings, these investigators recommend redesigning and optimizing new HVAC&R equipment specifically for these new refrigerants.

Regarding residential heat pump systems, R410A (GWP$_{100yr}$ of 2256) will be phased out in the coming years. Current suggested replacements for R410A are refrigerant blends included in the F-gas Regulations, such as R446A, R447A, R447B, R452B and R454B, among others. However, these potential replacements for R410A have GWP$_{100yr}$ values greater than 450 (IPCC AR6). Considering the future requirements for phasing out high-GWP refrigerants, investigating future refrigerants with GWP$_{100yr}$ <150 is crucial (EPA, 2021). In this study, R454C has been investigated as a potential low-GWP refrigerant replacement for R410A as its GWP$_{100yr}$ was estimated to be below the 150 threshold according to IPCC AR4 (148) and AR5 (146). Latest estimations published in the IPCC AR6 suggest that R454C has un updated GWP$_{100yr}$ of 166. However, R454C is not a direct drop-in refrigerant for R410A as it has lower volumetric capacity. Thus, a compressor with larger displacement was selected for R454C to try obtaining similar capacities as the baseline R410A system. This paper describes experimental comparisons that have been conducted under both heating and cooling modes. The effects of refrigerant charge amount and electrical valve opening were thoroughly investigated and are also presented. The results of this work can become a reference for performance analysis for R454C in R410A systems and could also provide insights into future system optimization studies.

2. CHARACTERISTICS OF WORKING FLUIDS

The zeotropic mixture R454C includes HFO-1234yf (A2L and GWP$_{100yr}$ of 0.501) and HFC-32 (A2L and GWP$_{100yr}$ of 771) in proportions of 78.5% and 21.5% (by mass), respectively. Table 1 provides a summary of thermophysical and transport properties of R410A and R454C for a direct comparison. The thermodynamic properties were retrieved from REFPROP library version 10.0 (Lemmon et al., 2018).

Table 1: Properties of R410A and R454C

Refrigerant	R410A	R454C
Composition, mass percentage	R32 (HFC): 50% R125 (HFC): 50%	R32 (HFC): 21.5% R1234yf (HFO): 78.5%
Normal boiling point, [a],℃	-51.44	-45.56
Critical temperature, ℃	71.34	85.67
Critical pressure, kPa	4,091.20	4,318.77
Molecular weight, g mol^{-1}	72.59	90.78
Latent heat of vaporization, [b], kJ kg^{-1}	273.09	227.51
Liquid cp, [c], kJ kg^{-1} K^{-1}	1.518	1.410
Vapor cp, [c], kJ kg^{-1} K^{-1}	1.130	0.975
Liquid density, [c], kg m^{-3}	1,169.95	1,136.31
Vapor density, [c], kg m^{-3}	30.57	20.53
Liquid thermal conductivity, [c], mW m^{-1} K^{-1}	103.43	86.16
Vapor thermal conductivity, [c], mW m^{-1} K^{-1}	12.45	11.90
Liquid viscosity, [c], μPa s	164.73	174.42
Vapor viscosity, [c], μPa s	12.03	10.92
Temperature glide, [b], K	0.0779	7.8043
Safety classification (ASHRAE 2016)	A1	A2L
ODP	0	0
GWP$_{100yr}$ (IPCC AR6)	2256	166

[a] At 1 atm; [b] At 100 kPa; [c] At 0 ℃

The critical temperature of R454C is approximately 14 °C higher than R410A. Thus, better performance of the system with the R454C at high ambient temperatures is expected. Referring to the saturated temperature and pressure relationship, R454C should operate at a lower pressure than R410A and has lower vapor density for expected compressor suction conditions. R454C also has lower specific heats and conductivities, which may cause negative effects on the heat exchanging process. The lower vaporization latent heat and vapor density leads to a lower capacity for the same compressor volumetric displacement rate at a given pressure when compared to R410A. Unlike pure fluids or azeotropic mixtures, R454C is a zeotropic mixture with a non-isothermal condensation or vaporization process because of the different boiling points of the individual components. At a constant pressure, zeotropic condensation begins at the dew point temperature and ends at the bubble point temperature. The difference between the dew point and bubble point temperatures is known as the temperature glide (T-glide). For example, at a pressure of 100 kPa, the temperature glide of R454C is 7.80 °C, much larger than that of R410A which is 0.0779 °C.

ANSI/ASHRAE 34 classifies the R454C in the 2L flammability group since its main components, R1234yf and R32, are also classified as 2L. Though it is difficult to ignite 2L gases, precautions must be taken to prevent accidental buildup of refrigerant, particularly during the charging of systems. Exhaust fan and leakage detective sensors are suggested during the charging process. The toxicity of R454C has been included in the toxicity group A "lower toxicity".

3. EXPERIMENTAL SETUPS AND TESTING

A fully-instrumented 10.5 kW (3RT) residential heat pump split system was installed in a pair of psychrometric chambers, as illustrated in Figure 1. The chamber can provide consistent conditions of temperature ($T_{dry-bulb} \pm 0.1$ °C), humidity (RH: ±0.5 %), air pressure and adequately mixed airflow to conduct repeatable experimental comparisons. The volumetric airflow rate of the air handling unit (AHU) was measured by a nozzle box designed according to ASHRAE Standard 37 (ASHRAE, 2005). The experimental setup, including system basic components, measuring devices and refrigerant piping, is shown in Figure 2. The system includes a fixed-speed scroll compressor (displacement of 29.55 cc/rev), fin-tube refrigerant-to-air evaporator and condenser, two electrical expansion valves (EXVs) with bypasses, one suction accumulator, several sight glasses and filter driers. As mentioned in Section 2, the thermophysical properties of R454C result in a lower volumetric capacity compared to R410A. Therefore, a fix-speed scroll compressor with larger displacement (44.4 cc/rev) was selected to better match the baseline R410A heat pump heating and cooling capacities. The temperature, pressure, mass flow rate of refrigerant, power consumption of compressor and fans were measured using thermocouples, pressure transducers, Coriolis-effect mass flow meter and wattmeter, respectively. In Figure 2, state points 1 to 8 are determined by measuring the temperature and pressure of the refrigerant. When operating in cooling mode, point 7 is used for observation but is not used in calculations, which is the same as point 4 in heating mode. Isenthalpic expansion is assumed across the electronic expansion valves (EXVs) and bypasses are used when expansion is not needed to avoid unwanted pressure drops. The uncertainties of measuring instruments are summarized in Table 2.
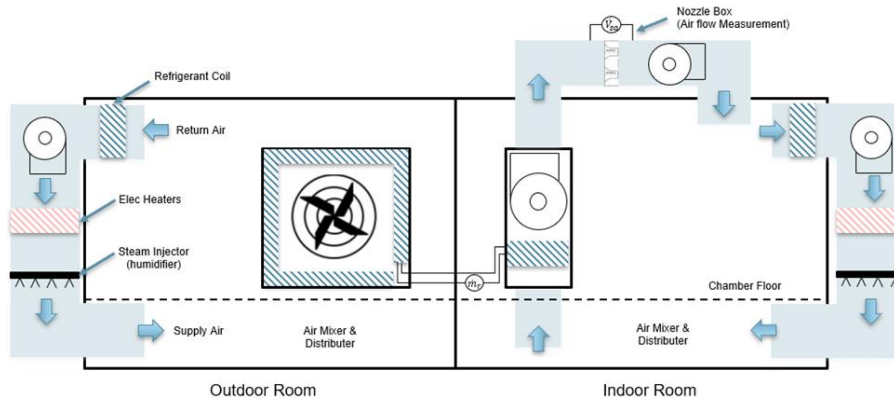

Figure 1: Psychrometric chamber schematic for setups

Table 2: Measuring instruments technical accuracy

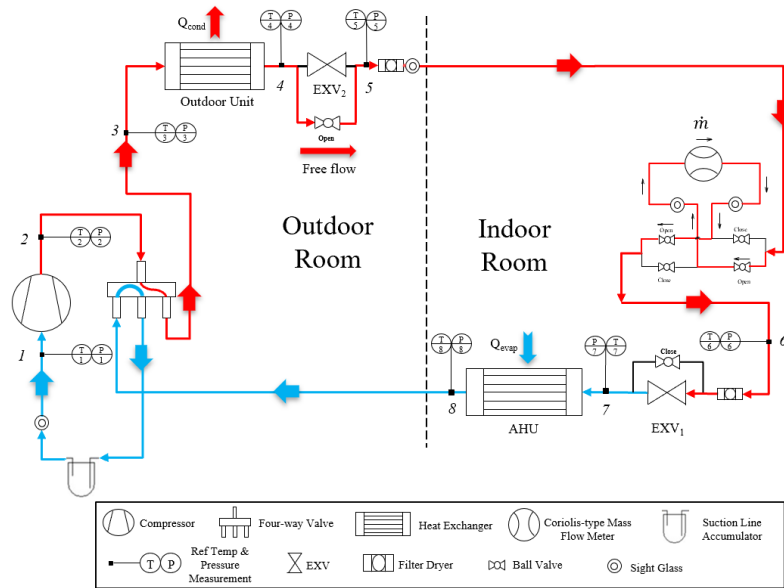| Instruments	Range	Accuracy (absolute or relative)
T-type thermocouple probe	-250~350 °C	± 0.5 °C
T-type thermocouple wire	-250~350 °C	± 1.0 °C
Pressure gauges	0~3447.37 kPa	± 0.13%
Chilled mirror dew point sensor	-35~25 °C	± 0.2 °C
Air differential pressure sensors	0~500 Pa	± 1.0% F.S.
Coriolis mass flow meter	0~315 g/s	± 0.1% F.S.
Wattmeter	0~4000 W (compressor) 0~200 W (outdoor fan) 0~1000 W (indoor fan)	±0.5% F.S.

Figure 2: The refrigerant system schematic of experimental setup (cooling mode flow as example)

The test conditions are listed in Table 3 and include standard rating conditions from AHRI Standard 210/240-2023 (AHRI, 2020) and extended outdoor conditions for testing system performance at high outdoor temperatures. The refrigerant charge level of R410A is based on the manufacturer's data and corrected to account for on-site pipe length to reach 5 °C subcooling temperature at the A_{full} condition. To consistently compare the cycle performance, charging sensitivity tests have been done for R454C to find refrigerant charge levels to match subcooling temperatures under the A_{full} and H_1 conditions. According to the test results, 4.30 kg and 6.75 kg of R454C were needed in heating mode and cooling mode, respectively. The evaporator outlet superheat temperature (SH) was controlled using EXVs and kept at 4 °C for all the conditions. The indoor AHU air flow rate was fixed at a nominal 1,100 CFM using a fixed speed fan motor.

Table 3: Testing conditions and cycle information

Mode		Outdoor Conditions		Indoor Conditions		Indoor air flow rate	R410A [a]		R454C [a]		SH, [c]
							charge level	SC, [b]	charge level	SC, [b]	
		dry bulb [°C]	wet bulb [°C]	dry bulb [°C]	wet bulb [°C]	[CFM]	[kg]	[°C]	[kg]	[°C]	[°C]
Cooling	**Ext₅**	46.11	32.64	26.67	19.44	1100	5.08	5.54	4.30	6.72	4.00
	Ext₄	43.89	30.80	26.67	19.44			5.43		6.45	
	Ext₃	41.67	29.13	26.67	19.44			5.30		6.21	
	Ext₂	39.44	27.39	26.67	19.44			5.21		5.96	
	Ext₁	37.22	25.56	26.67	19.44			5.12		5.61	
	A_full	35.00	23.89	26.67	19.44			4.98		5.31	
	B_full	27.78	18.33	26.67	19.44			4.03		4.63	
	C_full	27.78	14.44	26.67	13.89			4.66		4.36	
Heating	**H₁**	8.33	6.11	26.67	3.72			8.33	6.75	8.73	
	H₂	1.67	0.55	21.11	15.56			4.60		5.22	

[a] Scroll compressor displacement: 29.55 cc/rev (R410A); 44.4 cc/rev (R454C)
[b] SC: Condenser outlet subcooling degree
[c] SH: Evaporator outlet superheat degree

4. RESULTS AND DISCUSSIONS

4.1 Energy Balance

To ensure repeatability of the experimental data, each test was repeated at least two times at steady-state conditions. The refrigerant-side capacity is calculated from a first-law energy balance resulting in Equation (1).

$$\dot{Q}_{ref_{cooling}} = \dot{m}_{ref} \cdot \Delta h_{evap} = \dot{m}_{ref}[\, h_8(T_8, P_8) - h_6(T_6, P_6)]$$
$$\dot{Q}_{ref_{heating}} = \dot{m}_{ref} \cdot \Delta h_{cond} = \dot{m}_{ref}\,[h_8(T_8, P_8) - h_7(T_7, P_7)] \tag{1}$$

The net capacity of the refrigerant, assuming indoor fan power to be equal to the heat added to the air, is calculated as shown in Equation (2).

$$\dot{Q}_{net_{ref}} = \dot{Q}_{ref_{cooling}} - |\dot{W}_{fan}| \text{ (cooling)}$$
$$\dot{Q}_{net_{ref}} = \dot{Q}_{ref_{heating}} + |\dot{W}_{fan}| \text{ (heating)} \tag{2}$$

The air-side net capacity is calculated from a first-law energy balance across the indoor unit as shown in Equation (3). The enthalpy difference of the air (Δh_{air}) is calculated with measured dew point and dry-bulb temperature for supply air (SA, AHU outlet) and return air (RA, AHU inlet). The volume flow rate of the air ($\dot{V}_{air}$) is determined using a nozzle box connected to the ductwork of the indoor unit. The density of the air (ρ_{air}) is determined by the dry-bulb temperature at the nozzle box and the dew point temperature of the supply air.

$$\dot{Q}_{net_{air}} = \dot{m}_{air} \cdot \Delta h_{air} = \dot{V}_{air}\rho_{air}[h_{RA} - h_{SA}] \text{ (cooling)}$$
$$= \dot{V}_{air}\rho_{air}[h_{SA} - h_{RA}] \text{ (heating)} \tag{3}$$

The energy balances for R410A and R454C at different test conditions are displayed in Figure 3. Refrigerant- and air-side capacities were within 5% for all the test points, which is less than the ASHRAE Standard 37-2005 requirement of 6% (ASHRAE, 2005).
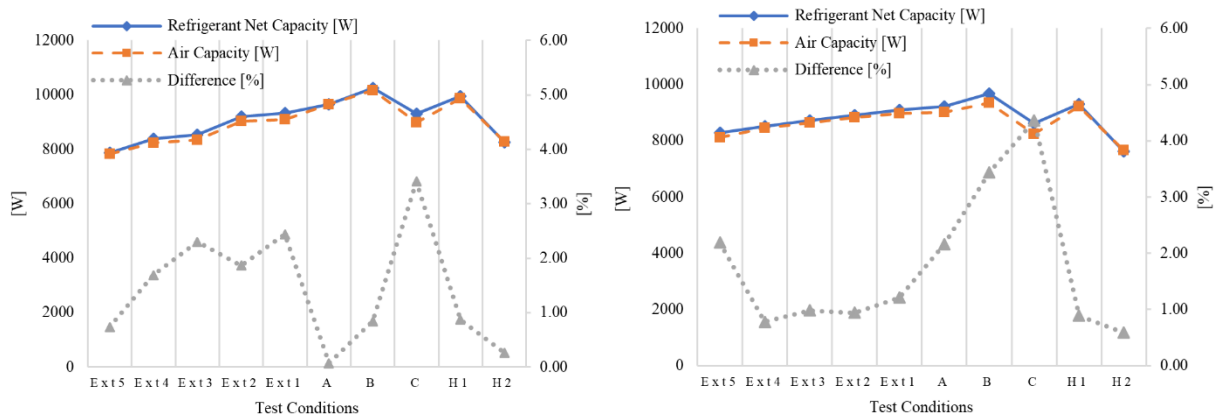

Figure 3: Energy balance for R410A (left) and R454C (right) at different test conditions

4.2 Heat pump performance comparison at different conditions

The system coefficient of performance (COP) is defined as the ratio of net cooling (or heating) capacity delivered to total power consumed by the compressor and fans.

$$COP = \frac{\dot{Q}_{net_{ref}}}{\dot{W}_{comp} + \dot{W}_{indoorfan} + \dot{W}_{outdoorfan}} \tag{4}$$

The system performance data at H_1 and H_2 conditions, including heating capacity, total power, mass flow rate and system COP are shown in Figure 4. When the outdoor temperature decreases (H_1 to H_2), for both fluids, the heating capacity, compressor power and COP decrease, which is mainly due to the reduced mass flow rate resulting from a lower refrigerant density at the compressor suction with lower evaporating temperature. Comparing the two fluids at two conditions, though the compressor with larger displacement could provide higher mass flow rate for R454C (5.08% for H_1 and 7.03% for H_2), R410A had 6.56% and 7.66% higher heating capacity than that of R454C. The lower heating capacity of R454C indicates that the increased mass flow rate cannot compensate for a smaller latent heat of vaporization at the condensing pressure compared to R410A. Additionally, the compressor for R454C has 1.93% and 4.01% higher power consumption due to its larger volume displacement. Finally, R454C has 8.37% and 11.36% lower COP compared to R410A at H_1 and H_2 conditions, respectively.
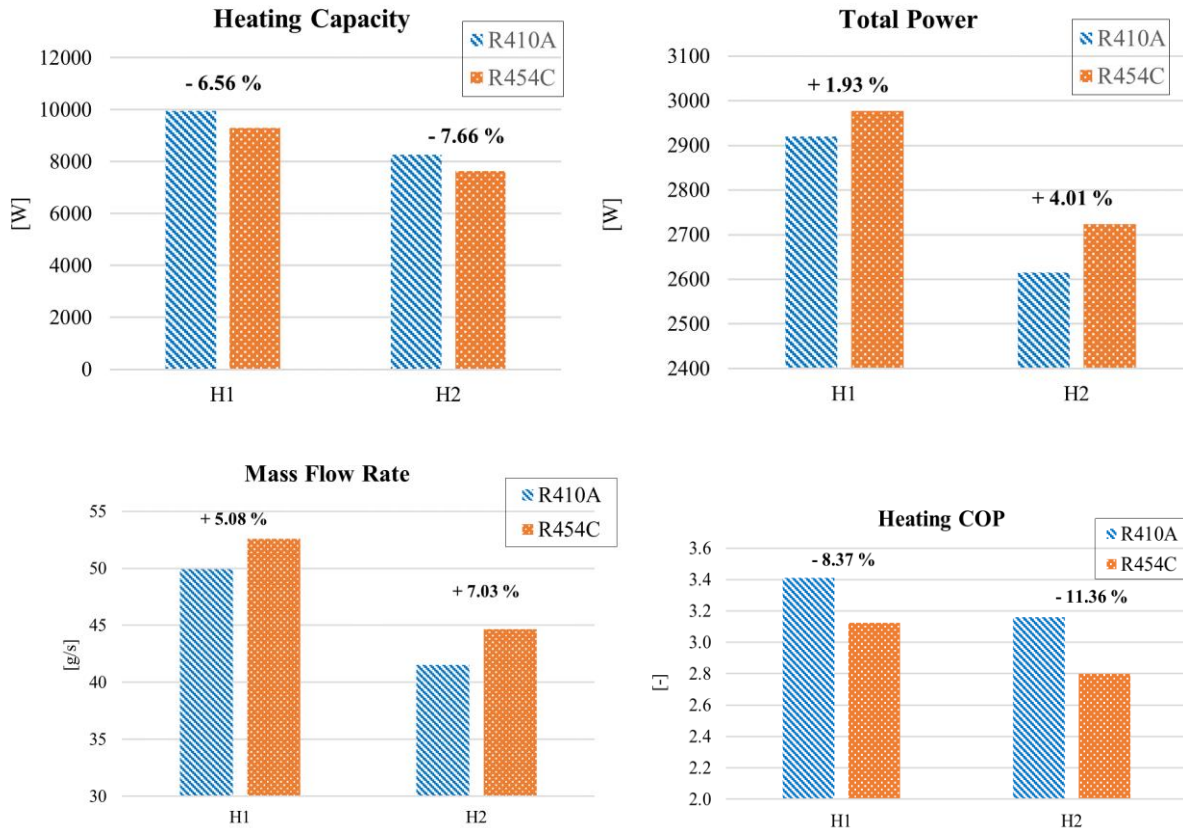
Figure 4: Heating performance for R410A and R454C at H_1 and H_2 conditions

The cooling performance of the unit with the two refrigerants under different conditions are compared in Figure 5. For both refrigerants, system cooling capacity decreases and compressor power increases as outdoor temperature rises. The enthalpy across the compressor (specific work) increases with larger pressure ratio, but mass flow rate would typically drop due to a lower volumetric efficiency. However, the increase in compressor specific work is more significant than the decrease in mass flow rate, which leads to increased compressor power consumption. Additionally, the increased evaporating inlet quality results in a lower enthalpy difference across the evaporator (i.e., lower refrigerating effect), which in combination with the lower mass flow leads to a lower cooling capacity. Furthermore, the lower refrigerating effect and higher compressor specific work lead to a lower cycle COP with higher outdoor temperature.

In most of the tested conditions, especially the AHRI Standard 210/240 conditions (*e.g.*, A and B), R410A showed superior performance compared to R454C, with greater cooling capacity, less power consumption and thus higher cooling COP. The higher capacity of R410A is likely due to a combination of a larger latent heat of vaporization that leads to improved evaporator heat transfer and poor flow geometry in the heat exchangers for the high-glide R454C

refrigerant. It is noteworthy that replacing the compressor with a higher displacement model led to mass flow rates that were higher than for R410A and yet the R454C system still had lower capacity. The higher compressor power of R454C compared to R410A is due to the higher mass flow rate for this larger displacement compressor as well as a lower overall isentropic efficiency. It is also noteworthy that the cooling capacity of R410A decreases dramatically from 10.2 kW to 7.8 kW (23%) when outdoor temperature increases from 27.78 °C (B) to 46.11 °C (Ext$_5$). On the contrary, R454C's cooling capacity only declines 14%, from 9.8 kW to 8.3 kW, outperforming R410A at Ext$_3$. It follows that R454C has better performance at warmer ambient conditions than R410A. Two main reasons can be attributed to such behavior. First, the latent heat of vaporization of R410A decreases significantly with the increase of the condensing pressure, i.e., at higher reduced pressure (P_{cond}/P_{crit}) values. The critical point of R454C is approximately 14 K higher than that of R410A and, thus, has a relatively larger latent heat of vaporization at the same pressures of R410A. Second, R410A has much higher reduced pressure values with higher outdoor temperature (*e.g.*, 0.82 at Ext$_4$ and 0.86 at Ext$_5$) than that of R454C (0.51 at Ext$_4$ and 0.54 at Ext$_5$). This leads to a more significant increase of pressure ratio and thus results in higher compressor specific work and decreased volumetric efficiency with lower mass flow rate. This also explains the reason that the cooling capacity and mass flow rate of R454C are less sensitive to the ambient temperature than R410A at the warmer ambient conditions.
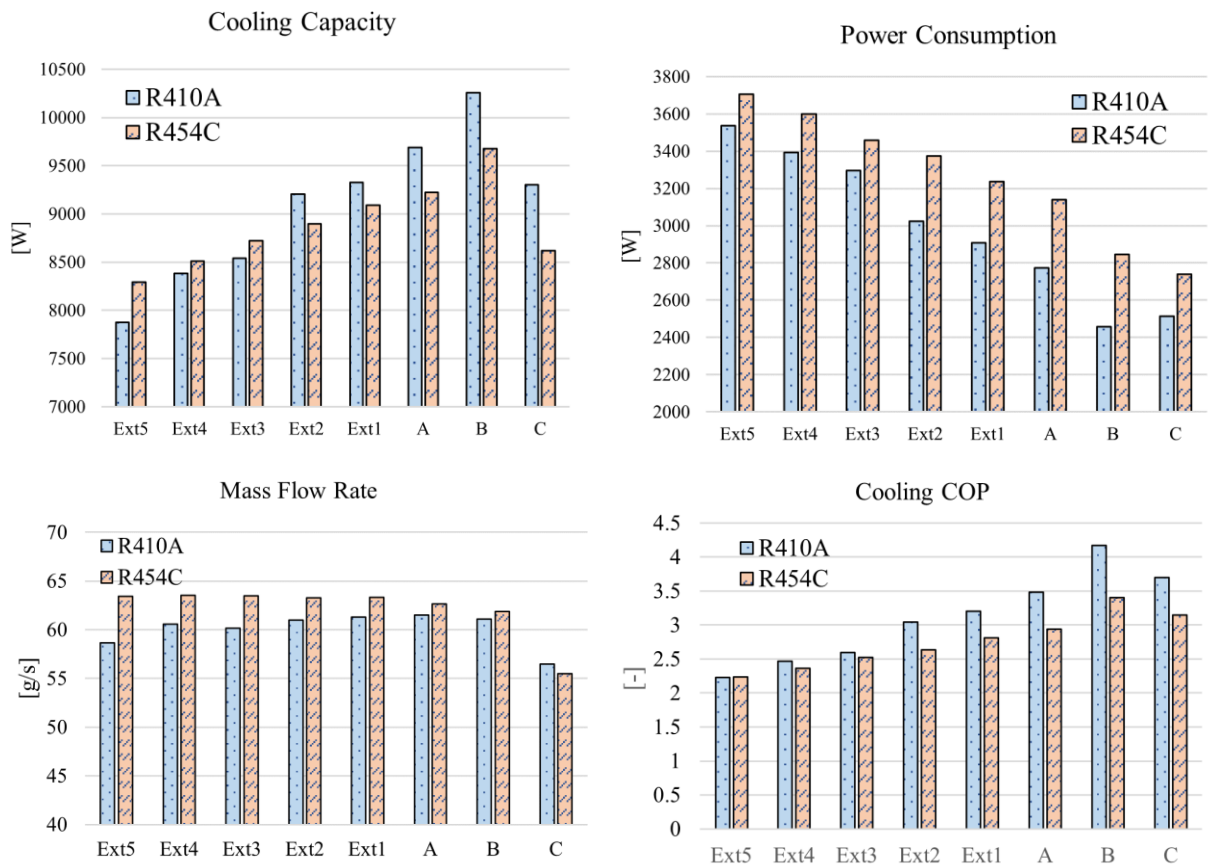

Figure 5: Cooling performance for R410A and R454C at AHRI and extended conditions

4.3 Effects of refrigerant charge and EXV opening on R454C experiments

The impacts of refrigerant charge on heat pump capacity and system performance vary for different units and operating conditions (Kim and Braun, 2010). An undercharged vapor compression cycle, which usually leads to high SH and low SC, can cause significant reductions in both cooling and heating capacity. Moreover, running equipment at an abnormally low charge level may also cause an increase of compressor discharge temperature and consequent overheating or triggering of a safety shutoff at an extreme high-pressure ratio, which could eventually shorten the unit lifespan. An overcharged heat pump may have low or no superheat and thus increases the compressor flooding risk. Meanwhile, the compressor consumes much more power as refrigerant is overcharged because the increased SC leads to a higher condensing pressure and thus higher compressor pressure ratio, which finally harms the system efficiency.

Charge [kg]	Mode	EXV safely operation range [%]															
		90	85	80	75	70	65	60	57.5	55	50	45	40	37	35	32.5	30
4.05	Heating	Two-phase into compressor				✓	✓	✓	✓	✓	✓	✓	Extreme high pressure ratio				
4.30							✓	✓	✓	✓	✓	✓	✓				
4.50								✓	✓	✓	✓	✓	✓	✓	✓	✓	
4.76									✓	✓	✓	✓	✓	✓	✓		
5.02		Charge Transition Zone: for heating mode, overcharged for cooling mode, undercharged															
5.31																	
5.57																	
5.98	Cooling	✓	✓	✓	✓	✓	✓	✓	✓	✓	✓	✓	Low capacity & COP				
6.28		✓	✓	✓	✓	✓	✓	✓	✓	✓	✓	✓	✓				
6.50		✓	✓	✓	✓	✓	✓	✓	✓	✓	✓	✓	✓	✓			
6.75			✓	✓	✓	✓	✓	✓	✓	✓	✓	✓	✓	✓			

Table 4: Charge sensitivity testing for R454C in R410A system

During the replacement process of R454C into the baseline R410A system, a large difference in the appropriate charge for heating and cooling modes was identified. To determine the proper charge levels of R454C, charge sensitivity tests were conducted under the H_1 condition (for heating) and A_{full} condition (for cooling), as shown in Table 4. This process started from an initial charge amount of 4.05 kg followed by the addition of about one-quarter kilogram charge at individual steps. At each refrigerant charge step, the EXV opening was controlled at a percentage to ensure that the system was running in a safe condition with proper SH and SC. The steady-state performance was then measured. The EXV was varied within a safe range to understand its impact on performance in combination with refrigerant charge variations.

As shown in Table 4, there is no overlap in refrigerant charge for cooling and heating modes at this test condition that can result in safe operation. Above a charge of 5.02 kg, the system is severely overcharged for heating and below a charge of 5.57 kg it is very uncharged for cooling. This charge transition zone depicted in Table 4 (5.02 to 5.57 kg) is where safe operation is not possible in either heating or cooling mode. This behavior means that R454C could not be a viable replacement refrigerant for this particular heat pump to realize a similar capacity as the baseline system with a single refrigerant charge without a redesign of the heat exchangers. Table 4 also shows how the range of safe EXV openings varies with refrigerant charge in heating and cooling modes. If the EXV opening is too large, then two-phase refrigerant can enter the compressor and potentially cause damage. On other hand, if the opening is too small then the pressure ratio will be too high which could damage the compressor in heating mode or result in very poor performance in cooling mode. It is interesting to note that cooling mode has a wider range of acceptable EXV openings than heating mode. This is due to lower pressure ratios and higher mass flow rates in cooling than heating mode.

In determining the charge levels that result in condenser subcooling to match the R410A baseline cycle, heating mode required 4.30 kg and cooling mode had a 6.75 kg charge. This large difference in charge requirements for heating and cooling mode is likely due to the heat exchanger capacity mismatches for this high-glide refrigerant. The refrigerant is in near counter-flow with air during the heating mode and in near parallel flow with air during the cooling mode. This high-glide refrigerant undoubtedly has better heat transfer performance with counterflow in heating mode than with parallel flow in cooling mode, because the refrigerant temperature glide is matched with the heat sink temperature glide (Zühlsdorf, 2018). Moreover, the larger displacement compressor that provides higher mass flow rate could amplify this heat exchanger capacity mismatch. These factors may explain why there is a significant difference in the charge requirements for heating and cooling that exists with this zeotropic mixture (R454C) that doesn't occur with the near-azeotropic mixture (R410A). Optimization of the heat exchangers and refrigerant flow pattern may be necessary to resolve this issue and obtain better performance with R454C.

Figure 6 shows the impact of charge level and EXV opening on the heating mode system performance that includes heating capacity, compressor power consumption, evaporator superheat and heating COP determined from testing at the H_1 condition. For the lower charge levels of 4.05, 4.30 and 4.50 kg, there was an optimum EXV opening that resulted in peak heating capacity. The heating capacity initially increases with EXV opening due to an increase of refrigerant mass flow rate that results in an improved condenser heat transfer. At EXV openings above the optimum, the heating capacity drops due to a decrease of the enthalpy difference across the condenser as superheat and

subcooling are decreased. The trend is different for the overcharged condition of 4.76 kg where the heating capacity does not approach a peak within the range of safe operation for the EXV. This is because the condenser enthalpy decrease is more significant than the increased mass flow rate as the EXV opening increases at this overcharged condition.

Figure 6 also shows that compressor power consumption increases with refrigerant charge for the smaller EXV openings but is relatively insensitive to charge at larger openings. The optimal refrigerant charge in terms of heating COP was the smallest charge considered in this work (4.05 kg). This charge level represents the best tradeoff in capacity and power consumption for this unit in heating. However, in order to match the heating capacity of the baseline R410A (9.96 kW) unit, a charge level of 4.76 kg was necessary. This led to a COP of 2.52 that was about 26% less than the baseline COP of 3.41 and about 18% less than the peak COP for R454C of 3.09 at a charge level of 4.05 kg.
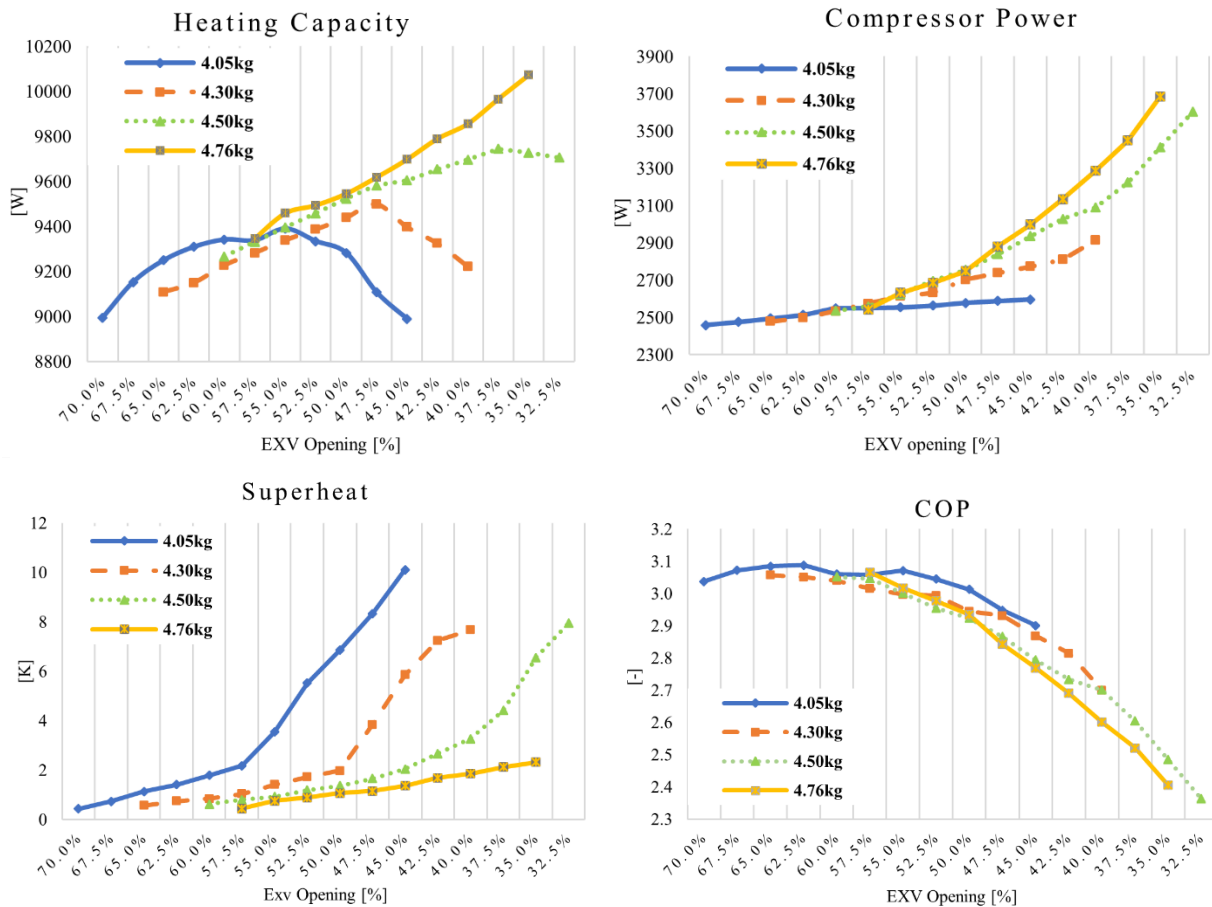

Figure 6: Heating charge sensitivity test results for R454C charge and EXV opening at standard H₁ condition

Figure 7 shows variation of cooling capacity, compressor power, evaporator superheat and cooling COP with refrigerant charge and EXV opening determined from testing at the A condition. Both cooling capacity and compressor power consumption increased with increasing charge over the range considered. However, COP was relatively insensitive to charge for the tested range with only a slight increase in COP at the larger charge levels. For each charge level, the cooling capacity, compressor power and cooling COP increased with increased EXV openings, which is mainly due to the higher mass flow rate. Different from heating mode, cooling capacity, power and COP in cooling mode had a relatively linear relation with the EXV openings and similar sensitivities among the different charge levels. For cooling mode, the best COP is achieved by minimizing the evaporator outlet superheat.

5. CONCLUSION

To evaluate the performance of R454C as a replacement for R410A, experiments on a 10.5 kW (3RT) residential split heat pump system were carried out for two working fluids at various operating conditions. A compressor with larger displacement was selected for R454C in an attempt to achieve a similar capacity as the baseline R410A system. The experimental results show that, though the compressor of R454C could provide higher mass flow rate, the capacity and efficiency of R454C system were lower than that of baseline system. In heating mode, the heating capacity and the system heating COP obtained with R454C were about 6.5~7.7% and approximately 8.4~11.4% lower than those for R410A, respectively. In cooling mode, the cooling capacity and the system cooling COP with R454C were about 2.5~10.6% and 6.9~21.2% lower than those obtained with R410A, respectively. In order to investigate the effects of refrigerant charge and EVX opening on the performance of the R454C system, sensitivity tests for both heating and cooling mode were conducted. Based on the experimental results, significantly different charges were identified for cooling and heating mode and there was no single refrigerant charge where the heat pump could operate safely in both cooling and heating modes. This behavior means that, without a redesign of baseline heat exchangers, R454C could not be a viable replacement refrigerant for this particular heat pump.
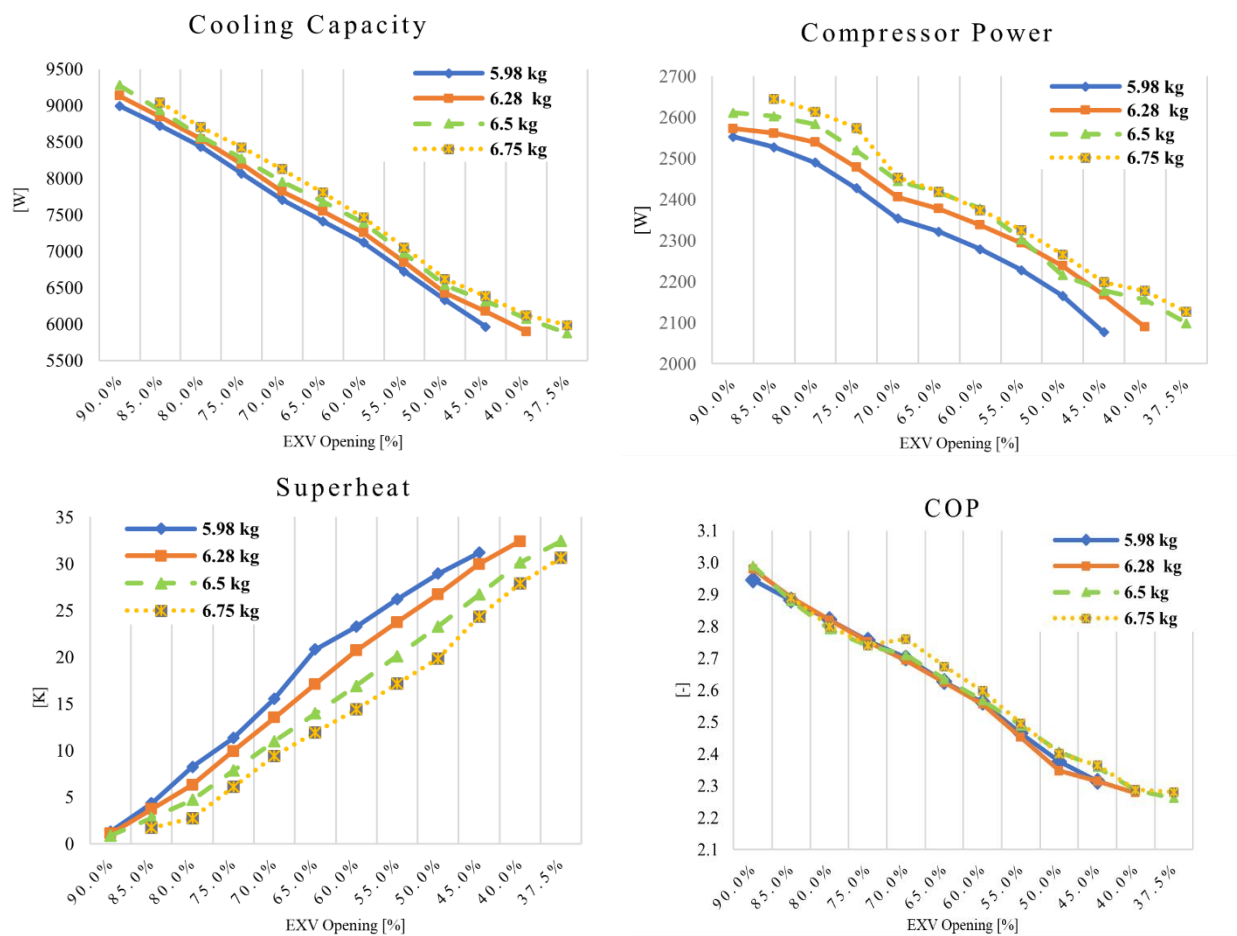
Figure 7: Cooling charge sensitivity test results for R454C charge and EXV opening at standard A condition

NOMENCLATURE

$\dot{Q}$	heat transfer rate	(kW)
$\dot{m}$	mass flow rate	(kg/s)
h	enthalpy	(kJ/kg)
$\dot{W}$	power	(kW)

| c_p | const. pressure specific heat | (kJ/(kg-K)) |

Acronyms

AHU	air-handling unit	EXV	electronic expansion valve
AR6	IPCC sixth assessment report	GWP	global warming potential
COP	coefficient of performance	ODP	ozone depletion potential
Ext	extended operation conditions	RT	refrigeration ton

Subscripts

comp	compressor	net_{air}	net of air
indoorfan	indoor fan in the AHU	cooling	cooling mode
outdoorfan	outdoor fan in the outdoor unit	heating	heating mode
net_{ref}	net of refrigerant	SA	supply air (AHU outlet)
		RA	return air (AHU inlet)

REFERENCES

AHRI. (2020). AHRI standard 540 for performance rating of positive displacement refrigerant compressors and compressor units (Standard). Arlington, VA, USA: Air-Conditioning, Heating, and Refrigeration Institute.

American Society of Heating, Refrigerating and Air-Conditioning Engineers. ANSI/ASHRAE Standard 34, designation and safety classification of refrigerants. 2016.

ASHRAE. (2005). ANSI/ASHRAE Standard 37-2005, Methods of Testing for Rating Electrically driven Unitary Air-Conditioning and Heat Pump Equipment. Atlanta: ASHRAE.

European Commission, 2014. Regulation (EU) No 517/2014 of the European Parliament and of the Council of 16 April 2014 on fluorinated greenhouse gases and repealing Regulation (EC) No 842/2006.

EPA, 2021. Final Rule - Phasedown of Hydrofluorocarbons: Establishing the Allowance Allocation and Trading Program under the AIM Act. https://www.epa.gov/climate-hfcs-reduction/final-rule-phasedown-hydrofluorocarbons-establishing-allowance-allocation.

Godwin, D. S., & Ferenchiak, R. (2020). The implications of residential air conditioning refrigerant choice on future hydrofluorocarbon consumption in the United States. Journal of Integrative Environmental Sciences, 17(3), 29-44.

Kim, W., & Braun, J. E. (2010). Impacts of refrigerant charge on air conditioner and heat pump performance.

Lemmon, E.W., Bell, I.H., Huber, M.L., McLinden, M.O. NIST Standard Reference Database 23: Reference Fluid Thermodynamic and Transport Properties-REFPROP, Version 10.0, National Institute of Standards and Technology, Standard Reference Data Program, Gaithersburg, 2018. doi: https://doi.org/10.18434/T4/1502528

Masson-Delmotte, V., Zhai, P., Pörtner, H. O., Roberts, D., Skea, J., Shukla, P. R., ... & Waterfield, T. (2018). Global warming of 1.5 C. An IPCC Special Report on the impacts of global warming of, 1, 1-9.

Mota-Babiloni, A., Navarro-Esbrí, J., Barragán-Cervera, Á., Molés, F., & Peris, B. (2015). Analysis based on EU Regulation No 517/2014 of new HFC/HFO mixtures as alternatives of high GWP refrigerants in refrigeration and HVAC systems. International journal of refrigeration, 52, 21-31.

Mota-Babiloni, A., Navarro-Esbrí, J., Makhnatch, P., & Molés, F. 2017. Refrigerant R32 as lower GWP working fluid in residential air conditioning systems in Europe and the USA. *Renewable and Sustainable Energy Reviews*, *80*, 1031-1042.

IPCC, 2022: Climate Change 2022: Impacts, Adaptation, and Vulnerability. Contribution of Working Group II to the Sixth Assessment Report of the Intergovernmental Panel on Climate Change [H.-O. Pörtner, D.C. Roberts, M. Tignor, E.S. Poloczanska, K. Mintenbeck, A. Alegría, M. Craig, S. Langsdorf, S. Löschke, V. Möller, A. Okem, B. Rama (eds.)]. Cambridge University Press. In Press.

Zühlsdorf, B., Jensen, J. K., Cignitti, S., Madsen, C., & Elmegaard, B. (2018). Analysis of temperature glide matching of heat pumps with zeotropic working fluid mixtures for different temperature glides. Energy, 153, 650-660.

ACKNOWLEDGEMENT